Available online at www.sciencedirect.com
SCIENCE DIRECT®
Journal of Power Sources 139 (2005) 342–350
JOURNAL OF POWER SOURCES
www.elsevier.com/locate/jpowsour

Defining high power EMD through porosimetry

Stuart M. Davis*, William L. Bowden, Thomas C. Richards

Gillette Advanced Technology Center, 37A Street, Needham, MA 02492-9120, USA

Received 22 June 2004; accepted 20 July 2004
Available online 13 September 2004

Abstract

High power electrolytic manganese dioxide (HPEMD), offers distinct performance advantages in alkaline-MnO_2 cells compared to the best conventional alkaline EMD materials previously available. Advantages are seen mainly on heavy continuous and heavy pulse drains. No comprehensive model to explain the chemical and structural basis for the improved performance of HPEMD has yet emerged. Hydrothermal electrolytic plating of EMD at 120–125 °C has given rise to several exceptional materials including two samples with excellent high power discharge performance. A systematic study of physico-chemical properties of all of the hydrothermally produced materials as well as commercial EMD samples, including HPEMD, has shown that superior high power performance is linked to porosimetry. By employing the needed plating conditions, one can produce a superior HPEMD material having BET area in the range 20–31 $m^2\,g^{-1}$ and simultaneously a micropore area (deBoer "*t*" method) greater than 8.0 $m^2\,g^{-1}$, all within the context of a typical pore volume of 0.035–0.050 $cm^3\,g^{-1}$ and a calculated meso–macropore radius greater than 32 Å (cylindrical pore model). A qualitative model explaining the need for a balance between BET area and micropore area is proposed. A possible explanation regarding the physico-chemical nature of the micropores and their relation to cation vacancies, as supported by stepped potential electrochemical spectroscopy (SPECS) investigations of heat treated EMDs, is given.

Keywords: Electrolytic manganese dioxide; EMD; High power; HPEMD; Micropores; Porosimetry

1. Introduction

Electrolytic manganese dioxide (EMD) is produced commercially by electrolysis of an aqueous solution of $MnSO_4$ and H_2SO_4. Chemically EMD is a complex inter-growth of the simpler phases pyrolusite and ramsdellite with twin defects, cation vacancies and Mn(III) sites.

This structure is commonly called γ–ε MnO_2 [1] and can be written, following the Ruetschi [2] formalism as:

$$Mn_{(1-x-y)}{}^{4+}Mn_y{}^{3+}\square_x O_{(2-4x-y)}(OH)_{(4x+y)}$$

where $\square$ is a vacancy in the Mn(IV) lattice. In this formula, protons are included to compensate the missing 4^+ charges due to the Mn(IV) vacancies and also the missing 1^+ charge, wherever a Mn(III) replaces an Mn(IV) in the manganese lattice. When $x = y = 0$ (no Mn(IV) vacancies, no Mn(III)), then the formula reduces to stoichiometric MnO_2. When γ–ε MnO_2 (EMD) is heated, protons are lost as water to the extent of 3–6% of the starting weight of the EMD. Physically, EMD is a dense solid with significant internal porosity leading to a high BET surface area (20–100 $m^2\,g^{-1}$). This stands in contrast to other cathode materials such as $LiCoO_2$ (used in Li-ion cells) with BET area of <1 $m^2\,g^{-1}$. Exhaustive investigations have sought to relate EMD battery performance to chemical and crystallographic structure but there has been far less study of the relationship of battery performance to EMD porosity.

HPEMD displays superior performance on heavy continuous and heavy pulse drains to high cut-off voltages. HPEMD can have a significant impact on the high power performance of AA and AAA alkaline batteries. Kerr McGee patent US 6,527,941 B2 [3] describes a process for producing "high power" EMD. According to the teachings of this patent the preferred conditions are: $H_2SO_4/MnSO_4$ ratio = 2:1–4:1 and simultaneously, current density (CD) = 2–4 A ft^{-2}. This

* Corresponding author. Tel.: +1 781 292 8534.
E-mail address: stuart_davis@gillette.com (S.M. Davis).

0378-7753/$ – see front matter © 2004 Elsevier B.V. All rights reserved.
doi:10.1016/j.jpowsour.2004.07.020

may be compared to typical commercial conditions for EMD plating which are: $H_2SO_4/MnSO_4$ ratio = 1:2 and CD = 5–6 A ft^{-2}. The Kerr McGee patent cites improved performance of AA alkaline cells on the 1W continuous drain.

Gillette patent US 6,585,881 B2 [4] describes a process for producing EMD in a pressurized cell at >110 °C. Under particular operating conditions, HPEMD can be obtained. Specific conditions, which have yielded HPEMD are given in Table 1.

Since the high power performance of both the Kerr McGee and Gillette materials are markedly better than ordinary EMD while the conditions under which they were synthesized are markedly different from each other, we may naturally ask what physical or chemical properties these two sets of EMD materials have in common? The purpose of this paper is to compare the physico-chemical properties of these two sets of materials, in particular, those relating to porosimetry, and to show that all other things being equal, what distinguishes a HPEMD from an ordinary EMD is the distribution of surface area between the micropores and the remaining meso–macropores of the EMD.

2. Experimental/materials and methods

Samples of commercial EMD were obtained directly from suppliers or from the IBA (International Battery Association) as "IBA Common Samples". All of these were commercial quality, prepared in high volume production, including two samples of Kerr McGee HPEMD.

The Gillette HPEMD samples, referred to here as EXP1 and EXP27 were prepared at the Gillette Advanced Technology Center, Needham in a hydrothermal electrolytic plating cell of our own design. A description of this cell has been presented at a recent congress [5] and a more detailed description will publish shortly in the full proceedings of the congress (in press). In summary, the plating cell consisted of a Teflon lined pipe spool with total volume of 16.1 l and working volume 11.6 l. Temperature could be adjusted in the range 100–150 °C and maintained to ±0.5 °C. Working pressure was upto 5 atm gauge. With the exception of trial EXP1, the cell was equipped with one Ti anode (two sides + edges = 535 cm^2) and two graphite cathodes (1 side = 355 cm^2). The cell electrolyte was continually refreshed during the plating trial and a constant electrolyte composition was maintained in the cell by balancing the plating current and pump speed. Approximately, 1.5 kg EMD was plated in each trial.

EXP1 constituted a "shakedown" trial for the equipment and different conditions were employed. The Ti anode had an area (2 sides + edges) of 91.1 cm^2 and the two graphite cathodes had an area (one side) of approximately 52 cm^2 Electrolyte was static and the quoted composition was the average for the 10-day trial, varying by ±15% around the nominal values. The key operating conditions for EXP1 and EXP27 are given above in Table 1, Section 1.

Electrolytic solutions were prepared with reagent $MnSO_4{\cdot}H_2O$ (Spectrum, ACS, M1115), reagent H_2SO_4 (Fisher, ACS, A300-212) and de-ionized H_2O. Final pH was adjusted as needed by small additions of $MnCO_3$ (Spectrum, ACS, M1100) or H_2SO_4. After pH adjustment the solutions were clarified by addition of small quantities of reagent H_2O_2 (Alfa Aesar, ACS, stock no. 33323).

The cell was filled with electrolyte having the desired operating composition. For all trials where circulating electrolyte was employed (EXP1 excepted) the pumping speed for the feed solution was balanced against the electrolysis current so as to maintain a constant composition within the cell. The manganese concentration in the feed solution was arbitrarily set at 150% of that for the cell electrolyte so that with a 33% stripping ratio, the desired manganese composition was maintained. The H_2SO_4 level in the feed was adjusted so that with 33% Mn stripping from the feed, the final desired level of acid was generated in the cell. Quality checks on the feed and effluent solutions consisted of regular monitoring for density, pH and conductivity using a glass hydrometer float, a Fisher Accumet pH meter (model 15) and a GLI International inductive conductivity probe (model 33, Cole Parmer cat. no. 19065-34). Two of these 3 variables are sufficient to define a unique composition of $H_2SO_4 + MnSO_4 + H_2O$. Through the use of previously constructed contour plots for paired variables we were able to conveniently monitor the H_2SO_4 and $MnSO_4$ levels and to cross check values obtained from one plot (e.g. density, conductivity) against another (e.g. density, pH). In the event that the effluent composition showed any sign of drifting, the pump speed was adjusted to bring it back to the desired values.

The EMD samples were "finished" by the conventional procedure of crushing in a steel jaw crusher, grinding in a steel "Shatterbox", water washing and neutralizing with NaOH to a constant pH of 5.0–6.0. Drying was done at 60 °C for 24 h in a forced convection oven with the powder contained in a glass tray. The maximum powder thickness was limited to 1.3 cm to insure easy escape of sorbed water. The powder cake was turned over once or twice during drying. (Temperature was limited to 60 °C in order to avoid any possible degradation of the EMD due to overheating.)

Porosimetry measurements were made on a Quantachrome 6 station Autosorb unit with N_2 gas. Prior to

Table 1
Plating conditions for two high power EMD samples in a pressurized cell

Trial	H_2SO_4 (M)	$MnSO_4$ (M)	$H_2SO_4/MnSO_4$ (ratio)	CD (A ft^{-2})	Temperature (°C)	Other
EXP1	0.63	0.88	0.72	6.19	120	Ti doped
EXP27	1.04	0.75	1.39	9.38	120	None

running the porosimetry measurements, samples were preconditioned at 150 °C for 7 h, under dynamic vacuum in the Quantachrome 6 station Degasser apparatus. Further details of the measurement procedure are given in Section 3.

3. Theory and calculation

Our object in this paper is to explain the high power performance of EMD in terms of porosimetry. Some terms employed in measuring and describing pore sizes are explained here following generally accepted definitions and the method used to calculate the average meso–macropore diameter according to a cylindrical pore model is derived. The construction of hypothetical plots of meso–macropore radius as a function of BET and micropore areas is explained.

As conventionally defined, micropores are those pores with diameter <20 Å. Mesopores are pores with diameters from 20–500 Å. Macropores are pores with diameters >500 Å. In our treatment we have grouped the meso and macropores together (i.e. pores with diameters >20 Å) and have referred to these as "meso–macropores".

Micropore area and volume can be measured according to various methods based on different adsorption models and their associated isotherms. We chose the deBoer "*t*" method [6]. Total surface area (BET area) was measured according to the classical Brunauer–Emmett–Teller method [7]. For the deBoer "*t*" method the relative pressure range employed in the calculation was P/P^0 = 0.1–0.5. For the BET method, the range was P/P^0 = 0.05–0.3. The calculations are performed automatically by the software supplied by Quantachrome. When the total surface area is measured according to the BET method, the micropore area is included in the measured BET area.

As part of our investigation, we constructed theoretical plots of average meso–macropore radius as a function of the BET area and the micropore area. The plots are based on the assumption of cylindrical pores all having a single valued average radius. The average meso–macropore radius is calculated according to the following equations:

$$\text{mM pore area} = \text{total BET area} - \mu\ \text{pore area} \quad (1)$$

$$\text{mM pore volume} = \text{total pore volume} - \mu\ \text{pore volume} \quad (2)$$

$$\text{mM pore volume} = (n)(l)(\pi)(r^2) \quad (3)$$

where n = number of pores in 1 gram

l = averge length of pores, r = average radius,

$$\text{mM pore area} = (n)(l)(2\pi r) \quad (4)$$

$$\text{mM pore volume}/\text{mM pore area} = r/2 \quad (5)$$

$$\text{mM pore radius} = r = 2(\text{mM pore volume})/(\text{mM pore area}) \quad (6)$$

where mM pore is the meso–macropore, μ pore the micropore. Micropore area and micropore volume were determined according to the deBoer "*t*" method, total pore volume was determined from the desorption isotherm according to the BJH (Barrett–Joyner–Hallenda) model [8].

For real samples, a physical measurement by the deBoer "*t*" method gives independent values both for micropore area ("*t*" plot slope) and micropore volume ("*t*" plot intercept). But, to construct a theoretical plot of meso–macropore radius as a function of total BET area and micropore area, we need a value for the micropore volume to include in Eq. (2), which is a function of the BET and/or micropore area.

In Table 4, we present measured porosimetry values (BET area, total pore volume, micropore area, micropore volume) for a series of 18 EMD and CMD (chemical manganese dioxide) samples.

For this group of materials we have noted that the measured micropore volume is roughly proportional to the measured micropore area according to the following relation:

$$\text{micropore volume}\ (\text{cm}^3\ \text{g}^{-1}) = 0.00047 \times \text{micropore area}\ (\text{m}^2\ \text{g}^{-1}) \pm 10\%$$

Since the micropore volume is typically only about 10% as big as the total pore volume, an error of 10% in estimating micropore volume will give only a 1% error in estimating meso–macropore volume when this approximation is employed in Eq. (2). If we assume a cylindrical pore model and any particular value for the total pore volume (micro + meso–macropores), then with the help of this approximation for micropore volume we can construct a theoretical plot of average meso–macropore radius as a function of two variables: BET area and micropore area (i.e. Eq. (6)). Two such "bubble plots" are presented in Fig. 1 for two different assumed values of the total pore volume.

In these plots we have arbitrarily distinguished between two ranges of calculated pore radii: Those with radii >32 Å (green) and those with radii less than 32 Å (red). The significance of this distinction will be seen later on. It should be noted that as the total pore volume is allowed to increase, for example from 0.035 to 0.040 $\text{cm}^3\ \text{g}^{-1}$, as shown here, the fraction of meso-macropores having average calculated pore radius >32 Å also increases (more green circles, fewer red circles).

4. Results

Physical and chemical properties for the two samples of HPEMD produced in the Gillette hydrothermal cell are compared to those for two commercial samples of Kerr McGee HPEMD and to some typical Kerr McGee standard EMD materials in Table 2.

Electrochemical performance in AA alkaline cells for the same HPEMD and standard EMD materials (shown above) is given in Table 3.

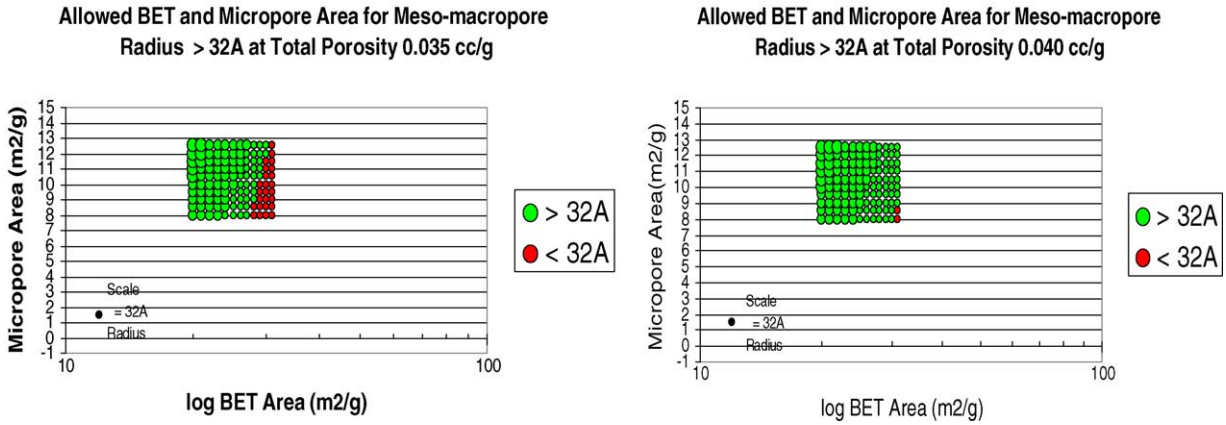

Fig. 1. Theoretical dependence of meso–macropore radius on BET and micropore areas.

Our control cells contained a 50/50 blend of KMHP with Std KM EMD. We did not run a control with 100% KM HPEMD in this series of tests. Broader experience has shown that the incremental performance gains achieved with 100% HPEMD versus a 50/50 blend are always less than the incremental gains achieved with a 50/50 blend compared to 100% of standard EMD. Based on this observation, we have estimated the upper limits of performance for 100% KM HPEMD as no more than 109% of control (to 1.1 V) and no more than 105% of control (to 0.9 V).

In Kerr McGee's patent US 6,527,941 B2 [3], they claim an 18% improvement in mWh on the 1W continuous drain for 100% KM HPEMD compared to 100% KM standard EMD (AA cells). This falls just below our limiting estimate for 100% KM HPEMD to 1.1 V, i.e. 109/91 = 19.7% relative improvement.

Another means of carrying out an electrochemical evaluation of our EMD samples, which avoids the laborious task of hand assembling a large number of AA cells, is to employ Bowden's SPECS coefficient as described in US Pats 6,440,181B1 [9] and 6,509,117 B1 [10]. SPECS stands for "Stepped Potential Electrochemical Spectroscopy", a technique originally developed by Chabre and Pannetier [1] to characterize EMD (and other cathode materials) via a slow, quasi-equilibrium stepped potential discharge. By measuring the peak power delivered at various discrete Voltage steps, Bowden was able to define a power coefficient = peak power at 1.4 V/peak power at 1.1 V, which correlates with the performance of a given EMD sample when it is discharged at high rate in a practical AA alkaline cell. The key parameters employed in measuring the SPECS coefficients of our EMD samples were as follows:

- Test vehicle: 635 coin cell with excess Zn anode
- Cathode: 30% graphite/70% EMD
- Electrolyte: 33% KOH, 2% ZnO
- Potential stepping rate: 5 mV h^{-1}

Employing the SPECS test to generate power coefficients for a series of 11 EMD samples and comparing these to the performance of the same EMD samples on the 1A continuous drain in AA alkaline cells, a good correspondence was obtained, in agreement with Bowden's earlier work. Plots of

Table 2
Comparison of high power EMD samples–physical and chemical properties

Sample	Gillette EXP1	Gillette EXP27	KM HPEMD (2 lots)	KM Standard EMD (typical)
MnO_x	1.98	1.98	1.98	1.92–1.96
Alk OCV vs. Zn (V)	1.69	1.69	1.66–1.67	1.60–1.65
SO_4^- (%)	1.58	1.81	1.13–1.15	1.0–1.2
True density (g cm^{-3})	4.34	4.39	4.40–4.44	4.4–4.6
"Q" ratio[a]	1.3	1.9	~1.0	0.6–0.7
BET area (m^2 g^{-1})	29.7	27.7	21.9–27.1	20–40
Ti (ppm)	2.160	64	7.8–18	10–15

[a] Cu Kα 22° peak/37° peak [6].

Table 3
Comparison of electrochemical performance for HPEMD and standard EMD samples in AA alkaline cells on the 1A continuous drain (as % of control)

Sample	Gillette EXP1	Gillette EXP27	100% KMHP	Control 50/50 KMHP/Std	100% KM Std EMD
Cut-off (V)					
1.1	135	123	<109 (est)	100	91
0.9	114	114	<105 (est)	100	95

Fig. 2. SPECS coefficient vs. AA cell performance on 1A continuous discharge.

the SPECS coefficient versus AA performance to 2 Voltage endpoints are shown in Fig. 2.

Having recognized that different EMD materials show significant differences with regard to micropore area, we attempted to correlate the electrochemical characteristics of the EMD with this parameter. In particular, we had observed that high power EMD materials always exhibited unusually high open circuit voltages (OCV), as seen in Table 1. Some high OCV materials however failed to give good high power performance. Conversely, no "standard" EMD had ever shown such a high alkaline OCV. Thus, high OCV could be considered "a necessary but not sufficient condition" for high power EMD. Plots were constructed of OCV versus micropore area and also versus the % micropore area, normalized to the total BET area, as in Fig. 3.

Correlations were observed in both cases, but a better correlation was obtained with %micropore area as opposed to absolute micropore area.

Similar plots were constructed for AA discharge performance (1A continuous drain) versus micropore area and % micropore area as in Fig. 4.

Again, a better correlation was observed with % micropore area compared to absolute micropore area. (The circled point is a projection for 100% KM HPEMD, as explained above.)

Finally, plots were constructed for SPECS coefficient versus micropore area and % micropore area as in Fig. 5.

Again, a better correlation was observed with % micropore area compared to absolute micropore area. Since performance and high OCV are seen to correlate better with % micropore area than absolute micropore area, we have concluded that high power EMD performance is linked to *both* the BET area and the micropore area. Following this conclusion we have plotted AA cell performance and SPECS results as bubble plots on a rectangular grid of BET area and micropore area, in Fig. 6.

Both the highest AA cell performance (1A continuous drain) and the highest SPECS coefficients are seen to fall within a "sweet spot" bounded by BET areas between 20 and 31 $m^2 g^{-1}$ and micropore area greater than about 8 $m^2 g^{-1}$.

When the samples of commercial EMD and CMD materials (Table 4) are compared to KM HPEMD and the two Gillette HPEMD samples on a similar plot, but with the calculated meso–macropore radii included, it is seen that this "sweet spot" corresponds to a region where the calculated radii are generally greater than 32 Å, as seen in Fig. 7.

In this plot, EXP1 and EXP27 are the two Gillette high power EMD samples, A is a Kerr McGee standard EMD

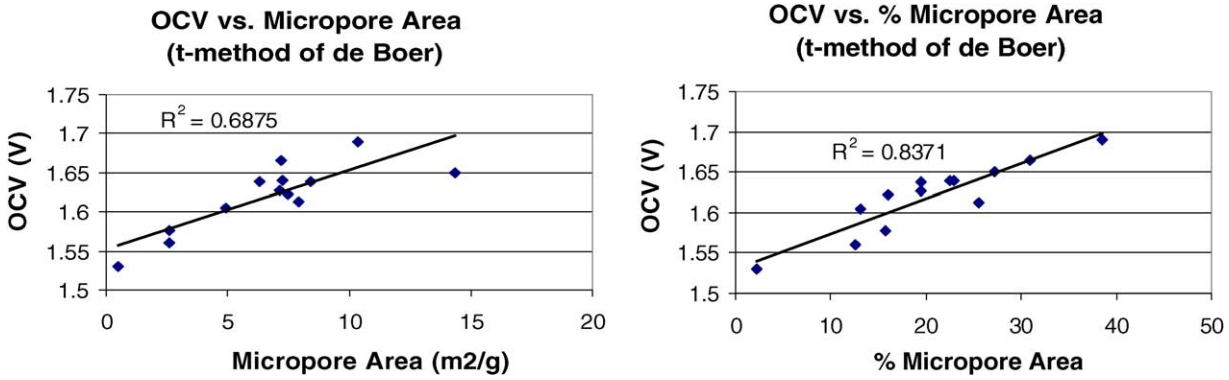

Fig. 3. OCV vs. micropore area and % micropore area.

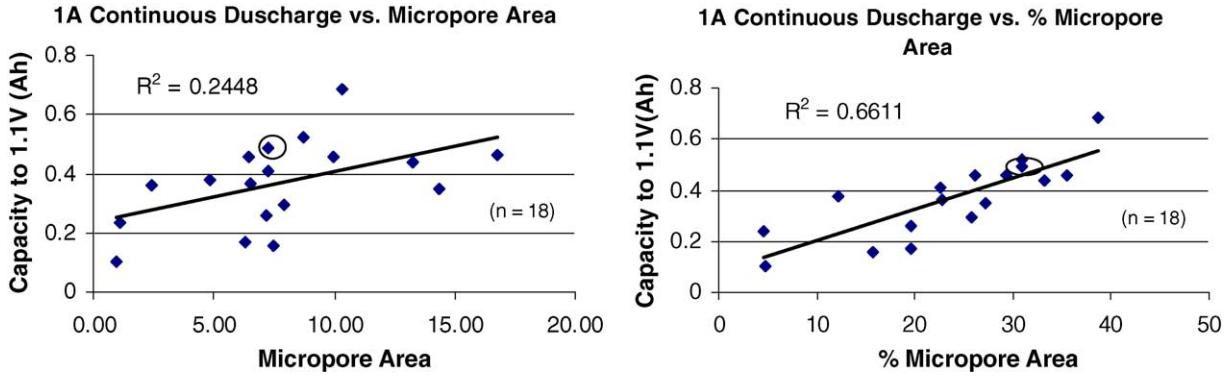

Fig. 4. AA cell performance vs. micropore area and % micropore area.

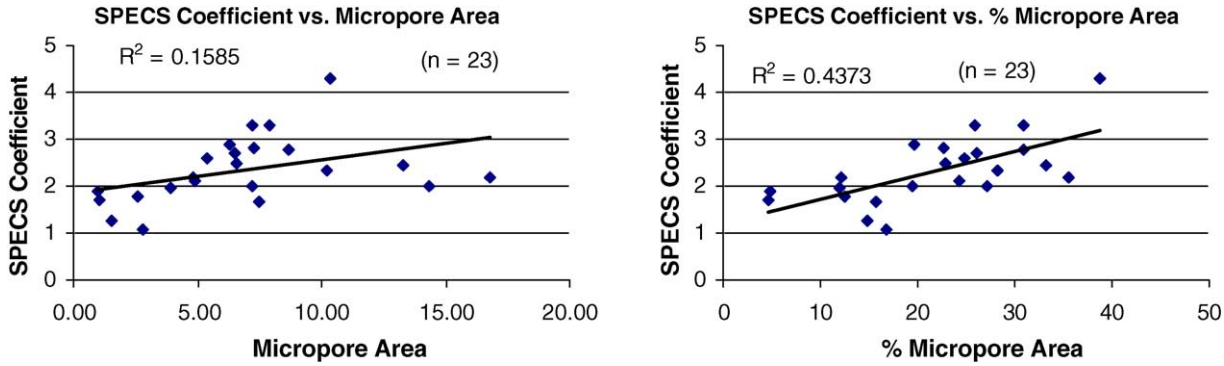

Fig. 5. SPECS coefficient vs. micropore area and % micropore area.

and B is a Kerr McGee high power EMD sample. (See Table 4 for remaining samples.) The parameters defining HPEMD by porosimetry are disclosed in US Pat Application 2003/0170170 A1 [11] as follows: BET area = 20–31 $m^2\,g^{-1}$, simultaneously micropore area = 8–13 $m^2\,g^{-1}$, simultaneously average calculated meso–macropore radius >32 Å, all within the context of a total EMD porosity of 0.035–0.050 $cm^3\,g^{-1}$.

Table 4
Measured porosimetry values for 15 EMD and 3 CMD samples

IC number or other ID	Sample name	BET area ($m^2\,g^{-1}$)	Micropore area ($m^2\,g^{-1}$)	Micropore volume ($cc\,g^{-1}$)	Intra-particle volume ($cc\,g^{-1}$)	Meso–macro pore radius (Å)
EXP1	EMD EXP1	26.74	10.31	0.00523	0.0372	38.87
EXP2	EMD EXP2	27.73	8.27	0.00361	0.0380	35.34
A	EMD KM Trona D	31.98	7.25	0.00367	0.0413	30.43
B	EMD KM HP	23.31	7.22	0.00366	0.0343	38.09
C	EMD Tosoh GHPT	25.64	0	0.00000	0.0423	33.00
D	EMD Tosoh HHP	40.87	8.83	0.00436	0.0516	29.49
E	EMD Chemetals	37.09	8.69	0.00428	0.0438	27.83
F	EMD Mitsui	30.37	4.06	0.00186	0.0453	33.01
10	EMD KM Trona D 6321	48.87	8.00	0.00370	0.0791	36.90
8	CMD Far M	92.46	0	0.00000	0.2023	43.76
22	CMD Japan 3/84	51.7	0	0.00000	0.1816	70.25
G	EMD Delta TL C878/I42	57.08	10.52	0.00499	0.0699	27.88
21	EMD	40.41	4.71	0.00227	0.1127	61.87
H	EMD KM Low Na 9864	45.55	9.58	0.00461	0.0567	28.96
12	CMD Synth MnO2 MHV	95.35	0	0.00000	0.1764	37.00
I	EMD KM TronaD Feb 02	26.98	5.46	0.00245	0.0388	33.74
J	XiangtanA Feb 02	34.94	6.03	0.00261	0.0499	32.70
K	XiangtanB Feb 02	43.92	11.54	0.00520	0.0488	26.91
				Avg→	0.0750	
				Median→	0.0499	

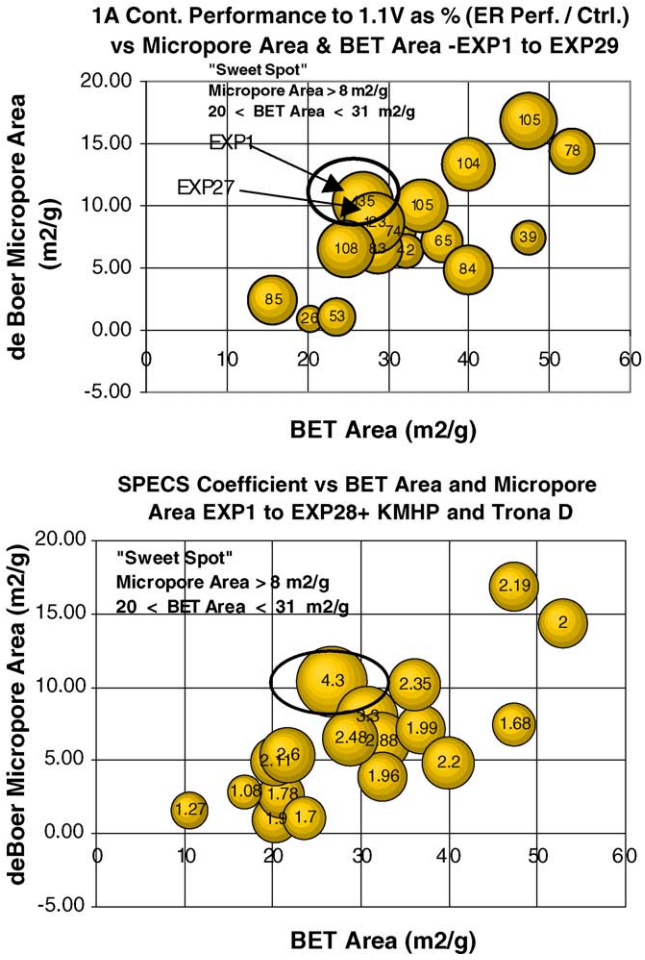

Fig. 6. Bubble plots of AA performance and SPECS coefficient vs. BET area and micropore area.

5. Discussion

As indicated in Section 3, when the total porosity of the EMD is allowed to increase beyond normal bounds (e.g. beyond 0.050 $cm^3\ g^{-1}$), more and more points on the grid will show a calculated meso–macropore radius >32 Å and the allowed upper bound for BET area can move to higher values. The downside of this approach comes when one wishes to produce a practical alkaline cell, within a limited volume. Then for high EMD porosity, the packing density of the EMD declines and the amount of active material which will fit within a given cathode volume becomes limited. Thus, a compromise must be struck between maximizing the micropore area, maximizing the meso–macropore radius and maintaining the packing density of the EMD.

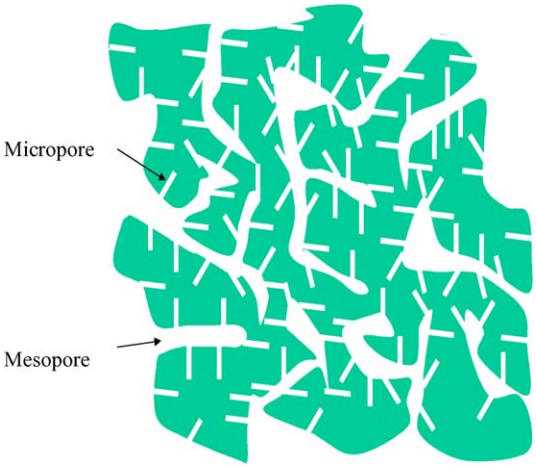

Fig. 8. Idealized MnO_2 particle with network of micropores and meso–macropores.

What has not yet been addressed is the reason that both high micropore area and a large average meso–macropore radius is needed for high power performance.

An idealized EMD particle with a network of interconnected micropores and meso–macropores is shown in Fig. 8.

It is believed that micropores are associated with both high OCV and fast discharge kinetics, i.e. high power capability, since a high micropore area is a requirement for HPEMD. It is also thought that the majority of micropores communicate to the bulk electrolyte through a network of meso–macropores. In this case, the overall electrode kinetics would be limited by the diffusion in the meso–macropores; specifically the

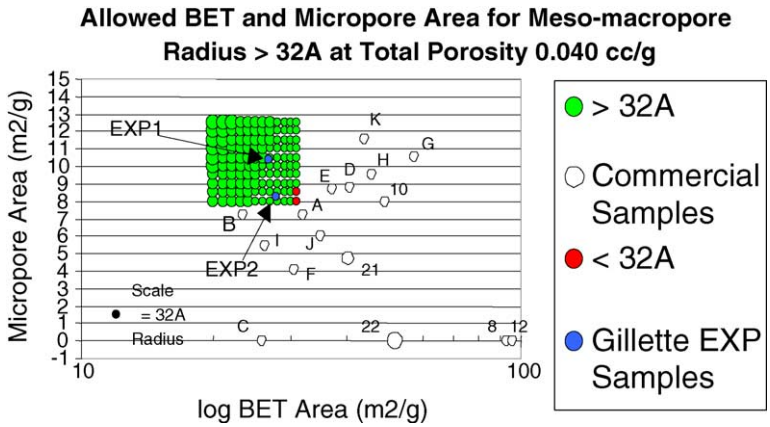

Fig. 7. EMD and CMD materials vs. BET area, micropore area and calculated meso–macropore radius.

diffusion of H_2O into the EMD particle and the diffusion of OH^- out of the particle, as required to support the cathode discharge reaction, as written in Eq. (7):

$$MnO_2 + H_2O + e^- \rightarrow MnOOH + OH^- \quad (7)$$

For a fixed total pore volume, the average meso–macropore diameter decreases as BET area increases. Thus, too high a BET area implies narrow pores, which are not favorable for diffusion. For a very low BET area, the pores may be large but there will simply be too few pores of limited extent, which is also unfavorable for diffusion. Thus, a middle range in BET area is required for good diffusion. At the same time, there must be a high micropore area to contribute high Voltage and fast kinetics, assuming that the diffusion limitation has been overcome in the meso–macropores.

This being said, we still have not addressed the question of the physical meaning or structure of the micropores. Porosimetry measurements are made on an EMD sample, which has been preconditioned by heating at 150 °C, in vacuum. A substantial quantity of H_2O is lost during this process, as much as 3–6% of the original sample weight. It is generally believed that this H_2O results from loss of cation vacancy protons along with an equivalent amount of oxygen, from the EMD lattice. We think that the measured micropores may represent the "fossil" remains of lost cation vacancy protons and their associated oxygen.

SPECS trials on heated EMD samples may be cited to support this interpretation. When a SPECS experiment is conducted on a normal EMD (not preheated) 5 distinct discharge processes can be identified at 5 characteristic Voltages. The highest voltage process occurs at 1.4 V (versus Zn) and shows the highest power (fastest kinetics) of all steps. The 1.4 V SPECS peak accounts for about 25% of the fresh discharge capacity and this is consistent with the reduction of all the Mn(IV) ions in nearest neighbor sites to the cation vacancies.

If the SPECS experiment is repeated with an EMD which, has been preheated at 150 °C, in vacuum, the fast 1.4 V process is absent. As is well known, the cation vacancy population and OCV are also irreversibly lowered by such heat treatment. Thus, it seems that the lost cation vacancies must have been the sites associated with high voltage and high power. But from porosimetry, it appears that the micropores are also associated with high Voltage and high power. Thus, it is not unreasonable to suggest that the micropores are associated with the cation vacancy sites and indeed may represent their remains, once they have been destroyed by heating.

If we use the cylindrical pore model to calculate the average micropore radius = 2(micropore volume)/(micropore area) for the 14 samples in Table 4 which show a measurable micropore area, this turns out to be 9.48 Å, substantially bigger than we might imagine arising from destruction of a single vacancy site. Thus there is an inconsistency in our interpretation. To salvage our idea about the origin of the micropores, we suggest the existence of vacancy clusters, formed either during the EMD deposition process or during the 150 °C preconditioning step for the porosimetry measurement. It is known that "annealing" and grain growth, with a consequent lowering of surface area, does occur when EMD is heated to higher temperatures, e.g. at 350 °C. So the idea that vacancies could diffuse and cluster together during heat treatment is not unreasonable.

Another curious aspect of the HPEMD prepared in our laboratory cell is its very high SO_4^- content, 1.58–1.9% (versus 1.2% for ordinary EMD). This is not simply a result of inadequate washing. No matter how thoroughly EMD is washed prior to neutralization there is always a residual SO_4^- content that remains. The SO_4^- appears to be well fixed in the crystal structure. That our highest performing HPEMD samples also show exceptionally high SO_4^- content seems more than coincidence.

Future investigations on the physical structure and origin of the micropores and the role of the "fixed" SO_4^- in HPEMD appear warranted.

6. Conclusions

HPEMD is distinguished by superior alkaline cell performance on both continuous and heavy pulse discharge. Based on a study of a series of experimental hydrothermally prepared EMD samples and comparisons to various commercial EMD and CMD materials we have found links between high power performance and porosimetry. Superior performance of HPEMD depends upon a balance of micropores and meso–macropores. Practical limits for these parameters are specified in terms of BET area and micropore area, thereby defining high power EMD. Widely different plating conditions may be employed to achieve high power EMD. A qualitative explanation is given regarding the relation of porosimetry to performance. We believe that the micropores measured by N_2 absorption after degassing at 150 °C represent the "fossil" remains of cation vacancies, which have been destroyed by heating. SPECS evidence has been cited to support this hypothesis. However, a comprehensive understanding of the links between EMD plating conditions, EMD structure and battery performance still eludes us.

Some additional points learned along the way, but not elaborated in this article due to lack of space and our desire to focus on porosimetry aspects, are as follows: high open circuit voltage is a necessary but not sufficient condition for obtaining HPEMD. Ti doping acts similarly to increased plating current density with regard to EMD properties and electrochemical performance. Higher Ti doping levels promote both higher BET area and higher micropore area. Ti doping is neither a necessary or sufficient condition for HPEMD. However, a HPEMD may be produced with a high level of Ti doping.

References

[1] Y. Chabre, J. Pannetier, Prog. Solid State Chem. (1995) 1–130.
[2] P. Ruetschi, J. Electrochem. Soc. 131 (12) (1984) 2737–2744.
[3] T.N. Andersen, S.F. Burkhardt, F.H. Wilmont Jr., R.F. Wohletz, V. Kazerooni, M. Reza, A.W. Unsell, US Patent 6,527,941 B2, March 4, 2003, Assignee: Kerr McGee Chemical, LLC.
[4] S.M. Davis, P.R. Moses, G. Miller, US Patent 6,585,881 B2, July 1, 2003, Assignee: The Gillette Co.
[5] S.M. Davis, Plating of high quality electrolytic manganese dioxide at 120–125 °C and 6X normal current density, in: Fifth International Symposium on New Materials for Electrochemical Applications, Montreal, Canada, July 6–11, 2003.
[6] J.H. deBoer, B.C. Lippens, B.G. Linsen, J.C.P. Broekhoft, A. vandenHeuval, Th.J. Osinga, J. Colloid Interf. Sci. 21 (1966) 405.
[7] S. Brunauer, P.H. Emmett, E. Teller, J. Am. Chem. Soc. 30 (1938) 309.
[8] E.P. Barrett, L.G. Joyner, P.H. Hallenda, J. Am. Chem. Soc. 73 (1951) 373.
[9] W. Bowden, K. Brandt, J.J. Cervera, H.S. Choe, R.A. Sirotina, J. Sunstrom, US Patent 6,440,181 B1, August 27, 2002, Assignee: The Gillette Co.
[10] W. Bowden, K. Brandt, J.J. Cervera, H.S. Choe, R.A. Sirotina, J. Sunstrom, US Patent 6,509,117 B1, January 21, 2003, Assignee: The Gillette Co.
[11] S.M. Davis, W.L. Bowden, P.R. Moses, T.C. Richards, US Patent Appl 2003/0170170 A1, September 11, 2003.